Thoughts on a new surgical assistance method for implanting the glenoid component during total shoulder arthroplasty. Part 1: Statistical modeling of the native premorbid glenoid

Julien Berhouet, Luc Favard, David Boas, Théo Voisin, Mohamed Slimane

Original article

Thoughts on a new surgical assistance method for implanting the glenoid component during total shoulder arthroplasty

Part 1: Statistical modeling of the native premorbid glenoid[1]

Julien **Berhouet** [1, 2, 3]*, Luc **Favard** [1, 3], David **Boas** [2], Théo **Voisin** [2], Mohamed **Slimane** [2]

[1] Université François Rabelais de Tours – Faculté de Médecine de Tours - CHRU Trousseau Service d'Orthopédie Traumatologie, 1C Avenue de la République, 37170 Chambray-les-Tours, France

[2] Université François Rabelais de Tours – Ecole d'Ingénieurs Polytechnique Universitaire de Tours – Laboratoire d'Informatique EA6300, Equipe Reconnaissance de Forme et Analyse de l'Image, 64 Avenue Portalis, 37200 Tours, France

[3] Western France Orthopedics Society (SOO) / HUGORTHO, 18, Rue de Bellinière, 49800 Trélazé, France

* Corresponding author: J Berhouet. Université François Rabelais de Tours - CHRU Trousseau Service d'orthopédie traumatologie 1C, Avenue de la République, 37170 Chambray-les-Tours, France

[1] Article issued from the Orthopaedics and Traumatology Society of Western France (SOO) – 2017 Tours meeting

Phone: 02 47 47 86 44

Fax: 02 47 47 59 12

Email: julien.berhouet@gmail.com

Acknowledgements: Christian Proust, PhD[2]

Abstract

Introduction: The aim of this study was to identify points on the scapula that can be used to predict the anatomy of the native premorbid glenoid.

Material and methods: Forty-three normal scapulas reconstructed in 3D and positioned in a common coordinate system were used. Twenty points distributed over the blade of the scapula (portion considered normal and used as a reference) and the glenoid (portion considered pathological and needing to be reconstructed) were captured manually. Thirteen distances (X) between two points not on the glenoid and 31 distances (Y) between two points of which at least one was on the glenoid were then calculated automatically. A multiple linear regression model was applied to calculate the Y distances from the X distances. The best four equations were retained based on their coefficient of determination (R^2) to explain a point on the glenoid being reconstructed ($p < 0.05$). In the first scenario, the glenoid was modeled assuming it was completely destroyed. In the second scenario, only the inferior portion of the glenoid was worn.

Results: For a completely destroyed glenoid, the mean error for a chosen distance for a given point on the glenoid was 2.4 mm (4.e-3 mm; 12.5 mm). For a partially damaged glenoid, the mean error was 1.7 mm (4.e-3 mm; 6.5 mm) for the same distance evaluated for a given point on the glenoid.

Discussion/Conclusion: The proposed statistical model was used to predict the premorbid anatomy of the glenoid with an acceptable level of accuracy. A surgeon could use

this information during the preoperative planning stage and during the actual surgery by using a new surgical assistance method.

Keywords: premorbid glenoid; multiple linear regression; statistical prediction; surgical assistance; shoulder arthroplasty

Introduction

Any surgical assistance method should allow the surgeon to refer to something visible as a reference, and to what is usually considered normal, so the surgeon can modify the procedure to correct the causative pathology. One example is the recent application of patient-specific guides (PSGs) in shoulder surgery, with the customized guides assisting with glenoid positioning. The PSG is secured to the glenoid, which is the only landmark visible to the surgeon. When PSGs are being designed, they incorporate the deformity correction from the preoperative plan, which is based on restoring normal anatomical parameters (version, inclination) (1-4). The limitations of PSG technology are that the surgeon uses the pathological glenoid to position the guide, which has variable amounts of wear and can be difficult to recognize in certain cases. At no point does the surgeon have a reliable, normal anatomical standard that could be used in case of technical difficulties. Moreover, no intraoperative criterion exists that can be used to assess the quality of the procedure carried out. This may result in a similar surgical scenario or can evolve into the situation the surgeon experienced before PSG technology was developed.

Preoperative and intraoperative visual information on the normal glenoid desired by the end of the surgery could be beneficial to the surgeon during the procedure. Another piece of intraoperative information—anatomical location and orientation of the whole scapula within its dense muscular envelope—would also represent meaningful progress for the surgeon's understanding and tracking in the surgical environment (5).

The end goal of providing the surgeon with intraoperative visual information on the appearance of the premorbid glenoid (i.e. state before it became worn) must go through a design process like the one used with PSG technology (2, 3, 6-9). Before customized guides are manufactured, a preliminary preoperative planning step is required that incorporates three-dimensional (3D) computed tomography (CT) reconstruction of the scapula (4, 9, 10). The

first step, namely modeling of the native or premorbid glenoid anatomy, must be completed before we can contemplate rebuilding a pathological glenoid into a normal one. The next step is transferring this information in the form of visual intraoperative assistance. The scientific challenge of restoring a normal glenoid resides in the fact that the information available about the glenoid at this preoperative step is, by definition, incomplete or even missing because of the glenoid's deterioration. The only normal anatomical structure usable at this stage is the blade of the scapula. These scapular landmarks, which are theoretically stable over time because they are not impacted by osteoarthritis, are the key to reconstructing the native glenoid. The aim of this first part of this work was to identify points on the scapula that can be used to predict the native premorbid glenoid anatomy using mathematical modeling with multiple linear regression techniques.

Materials and methods

1/ Materials

a/ Imaging of the scapula

Forty-three CT scans of normal glenohumeral joints were used in this project. The scans were preselected based on patient age and CT indication. Thus the CTs were from patients having an average age of 43.3 years (28–55 years). The CTs were initially ordered during the work-up of a polytrauma patient or a proximal humerus fracture. Each chosen CT was viewed and analyzed in its entirety to ensure the glenoid side of the joint was normal (no osteoarthritis, dysplasia or traumatic sequelae) and that the entire scapula was visible. These images were initially in DICOM format. They were imported into ImageJ® software to extract only the scapula in its entirety. The resulting files were in TIFF format. Lastly, the files were converted into OBJ format, so they could be used in the 3D imaging software chosen for all the portions of this research project: Blender®.

b/ 3D imaging software

Blender® (Blender Foundation, the Netherlands) is an open-source, 3D modeling, animation and rendering software. It has advanced modeling, 3D sculpting, texture mapping, special effects, 3D animation and rendering functions. Version 2.68a was used in this project.

With the Blender® software, the coordinates and center of an object were critical during the various experiments to ensure the same working coordinate system was used for each of the 43 manipulated scapula.

c/ Data processing and analysis software

We used the R® software in this project. This is open-source data processing and statistical analysis software implemented with the R programming language, which was itself inspired by Scheme (The R Foundation).

2/ Methods

The objective of modeling a native glenoid required several steps to be completed. The first was to construct a database with the set of 43 healthy scapulas. Linear regression techniques were then applied to model the native normal glenoid.

a/ Database

Precise manual pointing of each of the 43 normal scapulas reconstructed in 3D and placed in a common reference system was carried out with Blender®. Twenty points were captured by the surgeon. These points were chosen to be easily identifiable when they are selected on each scapula. A comparison of the pointing done by two, independent, non-surgeon raters was done beforehand to validate the reproducibility and precision of the process that will be repeated on the 43 scapula.

The points were distributed between the blade of the scapula, which was considered as normal over time and thus served as a reference, and the glenoid, which was considered as becoming pathological over time, thus a candidate for reconstruction. For each scapula in our study, a CSV (comma-separated value) spreadsheet was created to capture the coordinates (x,y,z) of each of the 20 points recorded. The following points were chosen, as shown on *Figure 1*:

- P_1: superior glenoid
- P_2: inferior glenoid
- P_3: most posterior point on glenoid
- P_4: most anterior point on glenoid
- P_5: most superior point on scapular blade
- P_6: most inferior point on scapular blade
- P_7: most medial point on scapular blade (or trigonum spinae)
- P_8: middle of the base of the spine projected on glenoid

- P_9: most posterior point on acromion

- P_{10}: most anterior point on acromion tip

- P_{11}: tip of coracoid process

- P_{12}: bottom of suprascapular notch

- P_{13}: junction of the pillar's anterior and posterior ridges

- P_{14}: anterosuperior pillar projected on glenoid

- P_{15}: posterosuperior pillar projected on glenoid

- P_{16}: inferior edge of base of spine projected on glenoid

- P_{17}: superior edge of base of spine projected on glenoid

- P_{18}: posterior edge of coracoid base projected on glenoid

- P_{19}: posterior edge of coracoid base projected on glenoid

- P_{20}: middle of coracoid base projected on glenoid.

With this set of points, the next step was to define 44 distances to be calculated, which corresponded to the variables needed to apply the regression methods.

- $X_{i,\,j}$ distances: 13 of them – the distance between two points, P_i and P_j, not on the glenoid. These distances were explanatory parameters, as they are unchanged even in a pathological glenoid. The following X distances were retained: $X_{5,6}$, $X_{5,7}$, $X_{5,10}$, $X_{5,11}$, $X_{6,7}$, $X_{6,9}$, $X_{6,11}$, $X_{7,9}$, $X_{7,10}$, $X_{7,12}$, $X_{9,10}$, $X_{10,11}$, $X_{11,12}$.

- $Y_{i,\,j}$ distances: 31 of them – the distance between two points, P_i and P_j, at least one of which was on the glenoid. These distances were variables to be explained, as they are used to reconstruct the glenoid shape, once a model has been chosen for each one. The following Y distances were retained: $Y_{1,2}$, $Y_{3,4}$, $Y_{1,7}$, $Y_{2,7}$, $Y_{3,7}$, $Y_{4,7}$, $Y_{7,8}$, $Y_{7,14}$, $Y_{7,15}$, $Y_{7,16}$, $Y_{7,17}$, $Y_{7,18}$, $Y_{7,19}$, $Y_{7,20}$, $Y_{2,13}$, $Y_{13,14}$, $Y_{13,15}$, $Y_{6,14}$, $Y_{6,15}$, $Y_{1,12}$, $Y_{2,12}$, $Y_{3,12}$, $Y_{4,12}$, $Y_{8,12}$, $Y_{12,14}$, $Y_{12,15}$, $Y_{12,16}$, $Y_{12,17}$, $Y_{12,18}$, $Y_{12,19}$, $Y_{12,20}$.

The distances chosen between points were calculated automatically using a tool developed in Java. This tool generated a matrix of 44 distances for each of the 43 scapulas or individuals. Several successive verifications of the matrix were performed to ensure there were no aberrant measurements or individuals.

b/ Application of multiple linear regression

The aim was to predict where each point is located on the glenoid based on its coordinates (*x, y, z*). Since these are obviously known beforehand, we could use this information to verify the consistency and accuracy of our predictive model. Since it is a 3D space, to find the coordinates of a glenoid point, we need to have four distances calculated from points with known coordinates. Thus, for each point, a local point-level model was composed of four distance equations. For example (Figure 2), to determine the coordinates of unknown point P_1, we needed the distance estimates P_1/P_{10}, P_1/P_{11}, P_1/P_7, P_1/P_{13}, with the coordinates for the points P_i, $\forall_i \neq 1$ are known. For each of these distances, a predictive equation was calculated; the entire set of these equations formed the local model at point P_1. The distances P_1/P_{10}, P_1/P_{11}, P_1/P_7, P_1/P_{13} were themselves estimated based on known distances (P_{10}/P_{11}, P_{10}/P_7, P_{10}/P_{13}, P_{11}/P_{13}…) during the use of multiple linear regression.

When applied specifically to the normal glenoid modeling project, the first regression problem was to identify the distances $X_{i,j}$ to be used to explain the distances $Y_{i,j}$. In the end, all of the possible Xi,j combinations were taken into account. The best combinations were then selected based on the highest possible coefficient of determination R^2, with a minimum of 0.75, a *p*-value below 0.05 and tests evaluating the squared residuals (Breusch-Pagan and Breusch-Godfrey tests). We decided to use up to four explanatory variables per equation.

The second problem was to identify, among the $Y_{i,j}$ distances to be explained (calculated), the best four equations to define the coordinates of the desired point P_i on the glenoid. We constructed a matrix of distances $Y_{i,j}$, $\forall j$ such that P_j was outside the glenoid. A

new script selected the best four statistically significant equations based on the values of the coefficient of determination, R^2.

This method was applied to characterize each point on the glenoid (Figure 1), except for points P_8 and P_{20} that we excluded because they were deemed redundant relative to neighboring points. In the first scenario, the glenoid modeling was done assuming the glenoid was completely destroyed. In practice, glenoid wear is most often localized, as evidenced by the classifications schemes of Walch *et al*. (11) and Favard *et al*. (12). Thus in the second scenario, the glenoid modeling was done assuming only the inferior portion of the glenoid was worn. The same regression methods were applied to only the points on the inferior portion of the glenoid, assumed to be missing because of inferior wear. Two new configuration files were tested in this second scenario. One contained the distance matrix with the $X_{i,\,j}$ identical to those of the first scenario, but with the $Y_{k,l}$ variables removed, including the upper *k* points on the glenoid, since the latter no longer needed to be determined. In the other, new X-type explanatory variables were added, corresponding to the new points, which are now known, on the superior portion of the glenoid: P_1, P_{16}, P_{17}, P_{18}, P_{19}. In this configuration, the Y-type distances involving these points, considered as “to be explained” in the first scenario tested, themselves became explanatory variables for the second modeling scenario (*fig 3*).

Results

1/ Equations

In the first scenario of a completely destroyed glenoid, the points P_5 and P_6 on the scapular blade were the best at predicting the coordinates of the glenoid points. The distances involving these points were always in the first two equations for modeling each point. The other points isolated in the other two equations for each model were more variable in their predictive ability. A portion of these results reporting the best four equations of distances $Y_{i,j}$ to be explained to characterize all of the glenoid points are provided in *fig 4*.

In the second scenario of a glenoid with inferior wear only, the introduction of new points with known coordinates, which were as close as possible to the destroyed glenoid being reconstructed using the new configuration files of distance matrix enriched with new "X" (i.e. $X_{q,5}$, $X_{q,6}$, $X_{q,7}$, with $q \in \{1, 16, 17, 18, 19\}$), led to a sensible improvement in the coefficients of determination, with confirmation of the relevance of points P_5, P_6 and the point P_7 (*fig 5*).

2/ Relevance of equations

Verification of the quality of the equations obtained for the two previously described models, on the scale of the 43 scapulas used in this project, was done by calculating the mean error induced by these equations using the root mean square deviation (residuals). In the completely destroyed scenario, the mean error for a chosen distance for a given point was 2.4 mm (4.e-3 mm; 12.5 mm). In the partially destroyed scenario, the mean error was 1.7 mm (4.e-3 mm; 6.5 mm) for the same distance evaluated for a given point; note that the number of points to predict was lower in this model. The mean error and its maximum value were cut in half relative to the first model.

Discussion

In this paper, we presented the complete process for developing a predictive model for a normal premorbid glenoid, which was based on a multiple linear regression method using a data set consisting of 43 healthy scapulas. The prediction accuracy of a given point on the glenoid ranged from 1.7 to 2.4 mm, depending whether part or all the glenoid needed reconstruction, and consequently the initial number of known points available as input for the statistical model.

The most important points to the prediction were the superior, inferior and medial (trigonum spinae) edges of the scapular blade. The latter two points had already been retained, with the center of the glenoid, to establish the reference anatomical coronal plane of the scapula (13). A scapular 3D axial or transverse reference plane was also defined, which was orthogonal to the prior one, passing through the medial point on the trigonum spinae and the glenoid center. These planes were initially defined to provide a reliable analysis method for glenoid anatomy. The scapular coordinate system created was independent of the position of the patient's shoulder or the orientation of the scapula during the examination, and consequently of its environment. It could be used to measure the defects in version and inclination of the pathological glenoid being corrected with a shoulder implant. Nevertheless, evaluating these descriptive glenoid criteria required us to define a reference plane for the glenoid itself. Several methods, two-dimensional (2D) and 3D, have been described (13-16). In addition to being tedious to implement, these methods are challenged when defining points of interest on the glenoid to reconstruct a plane, all the more in a pathological situation of wear or joint destruction.

More recently, 3D reconstruction and automatic segmentation software packages have been developed and made available to surgeons. These aim to allow accurate preoperative planning of a total shoulder arthroplasty procedure (4, 5, 17), and also to design PSGs used to

transfer and carry out intraoperatively the previously established plan. One of the most well-designed packages is the one developed by Imascap (Plouzané, France). This software, called Glénosys®, uses a least-square method to automatically created new scapular and glenoid planes, using all the 3D points on the scapula, no matter where the joint is damaged (17-19). In fact, it is based on these observations that this research project was implemented to develop a predictive statistical model for the premorbid glenoid. Beyond the description of the pathological glenoid, as is commonly done, our goal was to model the native glenoid. In practice, this is what surgeons hope to achieve when performing total shoulder arthroplasty. The surgeon attempts to use all the normal anatomical landmarks available, such as the blade of the scapula.

Prior knowledge of the anatomy of the premorbid glenoid being reconstructed could supplement the information provided by 3D planning and PSG design. The precision of the glenoid positioning with conventional manual instrumentation ranges from 7° to 11° for version and inclination. The accuracy for the placement of the entry point of the glenoid preparation pin when using PSGs is estimated to be 3 mm (1). When there is significant glenoid wear, with the need for a graft or augmented implant, we can presume the accuracy will be lower. When using PSGs, it is in fact the pin's entry point that is planned. When using a graft, this entry point no longer corresponds to the middle of the glenoid base plate when using a reverse shoulder implant. Intraoperatively, there is no way to verify the accuracy of the procedure carried out, or to go back to information about the desired correction objective. Thus it may be helpful for the surgeon to have a reconstruction of the premorbid glenoid available during the procedure.

The same ideas on the premorbid anatomy have also been discussed in the context of the proximal humerus (18). The problem of reconstructing the humeral epiphysis, especially in the trauma context, is comparable to that of correcting an arthritic glenoid. In fact, the anatomical landmarks are often missing and can make the fixation and implantation of the humeral prosthesis difficult or approximative.

Our study has several limitations. The first is related to its methods. All of the preliminary steps needed to develop the statistical model require manual imaging processing procedures (3D reconstruction, segmentation, capturing of points) with different software packages (ImageJ®, Blender®). Learning the various operations and mastering them may have contributed to imprecisions when putting together the initial database. An inter-rater reproducibility study was conducted to make sure the anatomical points captured on each scapula were relevant and precise.

Another limitation is the fact the accuracy of our statistical model was evaluated on only the 43 scapulas used to create the regression equations. In the end, this population served as its own control to evaluate the predictive method developed. It would have been interesting to test the equations developed on pathological cases, meaning scapulas with arthritic glenoids that are already worn and deformed. This is actually one of the methodological strengths of the project done to predict the premorbid anatomy of the proximal humerus. The statistical model developed was proven in cases of fracture and humerus defect (18).

Lastly, it would be interesting to test our prediction method on more complex descriptive features, such as version or inclination, instead of simply on glenoid points. In reality, this is the type of information that guides the correction and glenoid implantation strategy clinically.

Nonetheless, the approach used in the current study is relevant and original. Recent developments in 3D planning and PSG technology only provide partial information to support implant positioning, and on which the surgeon has no means of feedback during the procedure. The possibility of knowing the premorbid glenoid anatomy could constitute new preoperative and intraoperative information, helping the surgeon perform the needed correction and to select the implant features that are most suitable to the reconstructed anatomy.

Conclusion:

A statistical model to predict the premorbid anatomy of the glenoid was described in this article. This is new information for the surgeon, which could supplement the information provided by preoperative 3D planning and PSG design. The next challenge is to find and develop the medium by which this information will be made available and delivered to the surgeon. The emergence of augmented reality techniques is one potential surgical assistance means. This is the second avenue that will be explored and developed in part two of this project.

Conflict of interest: no conflict of interest relative to this study for any of the authors

Funding sources
None

Contribution
Julien Berhouet: main author, study designer and investigator
Luc Favard: study review
David Boas: data collection
Théo Voisin: data collection
Mohamed Slimane: design and review

References

1. Gauci MO, Boileau P, Baba M, Chaoui J, Walch G. Patient-specific glenoid guides provide accuracy and reproducibility in total shoulder arthroplasty. The bone & joint journal. 2016 Aug;98-B(8):1080-5. PubMed PMID: 27482021.

2. Hendel MD, Bryan JA, Barsoum WK, Rodriguez EJ, Brems JJ, Evans PJ, et al. Comparison of patient-specific instruments with standard surgical instruments in determining glenoid component position: a randomized prospective clinical trial. The Journal of bone and joint surgery American volume. 2012 Dec 5;94(23):2167-75. PubMed PMID: 23224387.

3. Heylen S, Van Haver A, Vuylsteke K, Declercq G, Verborgt O. Patient-specific instrument guidance of glenoid component implantation reduces inclination variability in total and reverse shoulder arthroplasty. Journal of shoulder and elbow surgery / American Shoulder and Elbow Surgeons [et al]. 2016 Feb;25(2):186-92. PubMed PMID: 26456430.

4. Iannotti J, Baker J, Rodriguez E, Brems J, Ricchetti E, Mesiha M, et al. Three-dimensional preoperative planning software and a novel information transfer technology improve glenoid component positioning. The Journal of bone and joint surgery American volume. 2014 May 7;96(9):e71. PubMed PMID: 24806017.

5. Berhouet J, Gulotta LV, Dines DM, Craig E, Warren RF, Choi D, et al. Preoperative planning for accurate glenoid component positioning in reverse shoulder arthroplasty. Orthopaedics & traumatology, surgery & research : OTSR. 2017 May;103(3):407-13. PubMed PMID: 28238965.

6. Levy JC, Everding NG, Frankle MA, Keppler LJ. Accuracy of patient-specific guided glenoid baseplate positioning for reverse shoulder arthroplasty. Journal of shoulder and elbow surgery / American Shoulder and Elbow Surgeons [et al]. 2014 Apr 13. PubMed PMID: 24739791.

7. Suero EM, Citak M, Lo D, Krych AJ, Craig EV, Pearle AD. Use of a custom alignment guide to improve glenoid component position in total shoulder arthroplasty. Knee surgery, sports traumatology, arthroscopy : official journal of the ESSKA. 2013 Dec;21(12):2860-6. PubMed PMID: 22932691.

8. Throckmorton TW, Gulotta LV, Bonnarens FO, Wright SA, Hartzell JL, Rozzi WB, et al. Patient-specific targeting guides compared with traditional instrumentation for glenoid component placement in shoulder arthroplasty: a multi-surgeon study in 70 arthritic cadaver specimens. Journal of shoulder and elbow surgery / American Shoulder and Elbow Surgeons [et al]. 2015 Jun;24(6):965-71. PubMed PMID: 25535020.

9. Wylie JD, Tashjian RZ. Planning software and patient-specific instruments in shoulder arthroplasty. Current reviews in musculoskeletal medicine. 2016 Jan 25. PubMed PMID: 26809956.

10. Iannotti JP, Spencer EE, Winter U, Deffenbaugh D, Williams G. Prosthetic positioning in total shoulder arthroplasty. Journal of shoulder and elbow surgery / American Shoulder and Elbow Surgeons [et al]. 2005 Jan-Feb;14(1 Suppl S):111S-21S. PubMed PMID: 15726070.

11. Walch G, Badet R, Boulahia A, Khoury A. Morphologic study of the glenoid in primary glenohumeral osteoarthritis. The Journal of arthroplasty. 1999 Sep;14(6):756-60. PubMed PMID: 10512449.

12. Sirveaux F, Favard L, Oudet D, Huquet D, Walch G, Mole D. Grammont inverted total shoulder arthroplasty in the treatment of glenohumeral osteoarthritis with massive rupture of the cuff. Results of a multicentre study of 80 shoulders. The Journal of bone and joint surgery British volume. 2004 Apr;86(3):388-95. PubMed PMID: 15125127.

13. Kwon YW, Powell KA, Yum JK, Brems JJ, Iannotti JP. Use of three-dimensional computed tomography for the analysis of the glenoid anatomy. Journal of shoulder and elbow

surgery / American Shoulder and Elbow Surgeons [et al]. 2005 Jan-Feb;14(1):85-90. PubMed PMID: 15723018.

14. Bryce CD, Davison AC, Lewis GS, Wang L, Flemming DJ, Armstrong AD. Two-dimensional glenoid version measurements vary with coronal and sagittal scapular rotation. The Journal of bone and joint surgery American volume. 2010 Mar;92(3):692-9. PubMed PMID: 20194328.

15. Bryce CD, Pennypacker JL, Kulkarni N, Paul EM, Hollenbeak CS, Mosher TJ, et al. Validation of three-dimensional models of in situ scapulae. Journal of shoulder and elbow surgery / American Shoulder and Elbow Surgeons [et al]. 2008 Sep-Oct;17(5):825-32. PubMed PMID: 18490182.

16. Budge MD, Lewis GS, Schaefer E, Coquia S, Flemming DJ, Armstrong AD. Comparison of standard two-dimensional and three-dimensional corrected glenoid version measurements. Journal of shoulder and elbow surgery / American Shoulder and Elbow Surgeons [et al]. 2011 Jun;20(4):577-83. PubMed PMID: 21324716.

17. Chaoui J, Hamitouche C, Stindel E, Roux C. Recognition-based segmentation and registration method for image guided shoulder surgery. Conference proceedings : Annual International Conference of the IEEE Engineering in Medicine and Biology Society IEEE Engineering in Medicine and Biology Society Annual Conference. 2011;2011:6212-5. PubMed PMID: 22255758.

18. Poltaretskyi S, Chaoui J, Mayya M, Hamitouche C, Bercik MJ, Boileau P, et al. Prediction of the pre-morbid 3D anatomy of the proximal humerus based on statistical shape modelling. The bone & joint journal. 2017 Jul;99-B(7):927-33. PubMed PMID: 28663399.

19. Moineau G, Levigne C, Boileau P, Young A, Walch G, French Society for S, et al. Three-dimensional measurement method of arthritic glenoid cavity morphology: feasibility

and reproducibility. Orthopaedics & traumatology, surgery & research : OTSR. 2012 Oct;98(6 Suppl):S139-45. PubMed PMID: 22964089.

Figure 1 : Image of the points picked on the scapula (sagittal view on the left and frontal view on the right).

Figure 2: Representation of the goal set for the multiple linear regression model. Schematic example of the determination of a point (P_1) on the glenoid from different scapular points located outside the glenoid (P_5, P_6, P_7, P_9, P_{10}, P_{11}, P_{13}). Four distance equations (P_1-P_{10}, P_1-P_{11}, P_1-P_7, P_1-P_{13}) were retained each time.

fig3: Configuration files of the distance matrix used for the regressions. On the left, the scenario of a completely destroyed glenoid. On the right, the scenario of a partially worn glenoid; the first configuration did not take into account the new variables X with the new points available on the upper glenoid, while the second configuration took them into account.

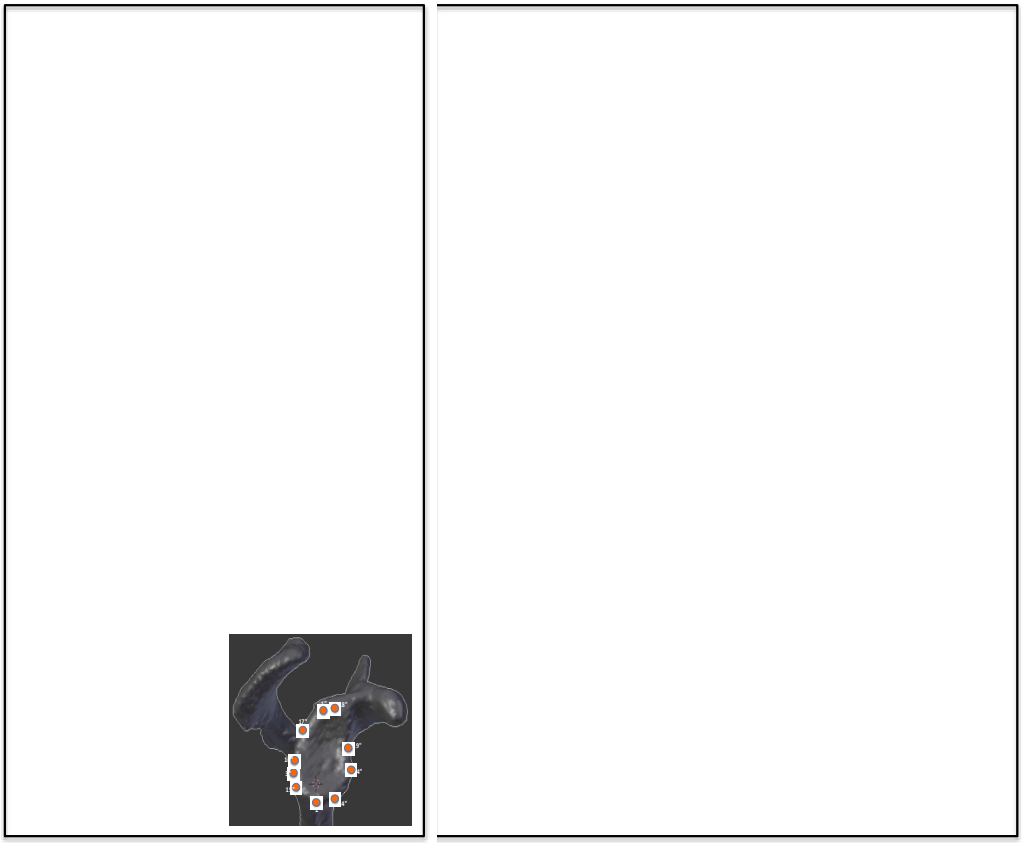

Fig 4: Examples of distance regression equations, with the best four explaining the points on the completely destroyed glenoid. The points P5 and P6 on scapular blade best predicted the coordinates of the points on the glenoid.

Equation P_1	Rsquared
Y1.5 = (0.244 X5.6) + (0.239 X6.11) + (-0.339 AngleA) + (-2.472 AngleE) + 366.497	0.95
Y1.6 = (0.201 X6.9) + (0.674 X6.11) + (0.382 X10.11) + (0.525 AngleE) + -76.875	0.94
Y1.7 = (-0.479 X5.10) + (0.383 X6.11) + (0.715 X7.10) + (-1.099 AngleE) + 151.761	0.86
Y1.10 = (0.447 X5.10) + (0.410 AngleA) + (0.657 AngleE) + (0.245 AngleFG) + -141.296	0.75

Equation P_2	Rsquared
Y2.5 = (0.500 X5.7) + (0.589 X6.7) + (-2.890 AngleE) + 408.586	0.96
Y2.6 = (0.330 X5.10) + (0.290 X6.9) + (1.809 AngleE) + (-0.541 AngleFG) + -173.832	0.94
Y2.7 = (-0.682 X5.10) + (0.403 X6.7) + (0.918 X7.10) + (-1.901 AngleE) + 276.369	0.91
Y2.10 = (0.247 X6.9) + (0.485 X9.10) + (-0.455 AngleE) + (0.238 AngleFG) + 45.285	0.73

Equation P_3	Rsquared
Y3.5 = (0.373 X5.7) + (0.382 X5.10) + (0.238 X6.9) + (-1.187 AngleE) + 160.582	0.87
Y3.6 = (-0.296 X5.11) + (0.640 X6.7) + (0.341 X7.9) + (-0.735 AngleFG) + 91.232	0.79
Y3.7 = (-0.622 X5.10) + (0.261 X6.7) + (0.953 X7.10) + (-1.616 AngleE) + 236.267	0.82
Y3.11 = (0.201 X5.7) + (0.271 X5.10) + (0.231 X6.9) + (-0.332 X7.9) + 18.987	0.66

Equation P_4	Rsquared
Y4.5 = (0.300 X5.7) + (0.509 X6.7) + (-2.110 AngleE) + (-0.384 AngleFG) + 329.723	0.91
Y4.6 = (-0.395 X5.11) + (0.595 X6.7) + (0.445 X7.10) + (-0.791 AngleFG) + 88.917	0.79
Y4.7 = (0.255 X5.10) + (0.961 X7.12) + (0.314 AngleA) + (0.742 AngleE) + -109.212	0.88
Y4.9 = (0.356 X6.9) + (0.315 X9.10) + (-0.700 AngleE) + (0.310 AngleFG) + 64.842	0.73

Equation P_{14}	Rsquared
Y14.5 = (0.399 X5.7) + (0.429 X6.7) + (0.240 X6.11) + (-2.592 AngleE) + 348.634	0.96
Y14.6 = (0.540 X5.10) + (0.412 X10.11) + (2.350 AngleE) + (-0.493 AngleFG) + -243.052	0.71
Y14.7 = (0.321 X5.6) + (-0.218 X5.7) + (-0.251 X6.9) + (0.580 X7.9) + 39.728	0.72
Y14.11 = (0.214 X5.7) + (0.276 X5.10) + (0.199 X6.9) + (-0.290 X7.9) + 20.720	0.62

Equation P_{15}	Rsquared
Y15.5 = (0.419 X5.7) + (0.299 X5.11) + (0.430 X6.7) + (-1.987 AngleE) + 274.890	0.92
Y15.6 = (-0.490 X5.10) + (0.520 X6.7) + (0.741 X7.10) + (-0.718 AngleFG) + 58.538	0.73
Y15.7 = (-0.827 X5.10) + (0.447 X6.7) + (1.106 X7.10) + (-2.131 AngleE) + 291.169	0.76
Y15.9 = (0.173 X5.7) + (0.398 X6.9) + (-0.967 AngleE) + (0.388 AngleFG) + 95.403	0.65

Equation P_{16}	Rsquared
Y16.5 = (0.282 X5.7) + (0.426 X5.10) + (0.278 X6.7) + (-1.439 AngleE) + 199.377	0.87
Y16.6 = (0.375 X5.10) + (0.359 X6.9) + (1.794 AngleE) + (-0.427 AngleFG) + -181.797	0.83
Y16.7 = (0.221 X6.7) + (-0.338 X6.9) + (0.783 X7.9) + (-0.260 AngleFG) + 53.564	0.72
Y16.11 = (0.181 X5.6) + (0.171 X5.10) + (-0.139 X7.9) + (0.260 X10.11) + 13.033	0.70

Equation P_{17}	Rsquared
Y17.5 = (0.290 X6.7) + (0.361 X7.10) + (-0.436 AngleA) + (-2.200 AngleE) + 329.887	0.87
Y17.6 = (-0.369 X5.11) + (0.700 X6.7) + (0.416 X7.10) + (-0.789 AngleFG) + 89.183	0.84
Y17.7 = (0.306 X5.6) + (0.181 X5.11) + (-0.255 X6.7) + (0.314 X7.9) + 32.674	0.76
Y17.10 = (-0.195 X5.6) + (-0.114 X5.11) + (0.254 X6.7) + (0.433 X7.10) + -10.42796	0.71

Equation P_{18}	Rsquared
Y18.5 = (0.247 X5.7) + (0.426 X6.7) + (-2.181 AngleE) + (-0.458 AngleFG) + 346.215	0.91
Y18.6 = (0.552 X6.9) + (0.493 X9.10) + (0.430 X10.11) + (-0.474 AngleA) + 46.789	0.89
Y18.7 = (0.341 X5.6) + (0.197 X5.11) + (-0.272 X6.7) + (0.238 X7.9) + 37.793	0.77
Y18.10 = (0.136 X5.10) + (0.476 X7.10) + (-0.446 X7.12) + (0.228 AngleFG) + -24.988	0.71

Equation P_{19}	Rsquared
Y19.5 = (0.386 X5.11) + (0.214 X6.9) + (0.432 X9.10) + (-1.241 AngleE) + 165.414	0.84
Y19.6 = (-0.485 X5.11) + (0.641 X6.7) + (0.514 X7.10) + (-0.827 AngleFG) + 92.234	0.82
Y19.7 = (-0.524 X5.10) + (0.347 X6.11) + (0.713 X7.10) + (-1.107 AngleE) + 161.645	0.69
Y19.10 = (0.458 X5.10) + (0.353 AngleA) + (1.149 AngleE) + -183.2155	0.57

Fig 5*:* Examples of distance regression equations, with the best four explaining the points on the partially destroyed glenoid. The points P_5, P_6, and P_7 on the blade of the scapula best predicted the coordinates of the points on the glenoid.

Equation P_2	Rsquared
Y2.5 = (0.578 X5.6) + (0.0738 X17.7) + (-2.254 AngleE) + 318.767	0.996
Y2.6 = (0.549 X17.6) + (0.377 X19.6) + (0.407 AngleA) + -27.184	0.95
Y2.7 = (0.219 X6.7) + (0.800 X1.7) + (0.493 AngleA) + -24.922	0.94
Y2.9 = (0.317 X5.6) + (0.368 X6.9) + (-0.567 X17.5) + (-1.772 AngleE) + 236.052	0.72

Equation P_3	Rsquared
Y3.5 = (0.334 X5.7) + (0.288 X6.7) + (0.536 X1.5) + (-1.248 AngleE) + 171.124	0.95
Y3.6 = (-0.297 X5.6) + (0.502 X16.5) + (0.884 X17.6) + (1.265 AngleE) + -168.419	0.93
Y3.7 = (0.141 X6.7) + (1.048 X17.7) + (-0.314 X18.5) + (-0.723 AngleE) + 105.440	0.94
Y3.9 = (-0.129 X5.11) + (0.619 X6.9) + (-0.426 X16.6) + (-0.386 AngleE) + 57.224	0.78

Equation P_4	Rsquared
Y4.5 = (0.449 X5.6) + (-0.157 X5.7) + (0.377 X18.7) + (-1.875 AngleE) + 251.036	0.95
Y4.6 = (0.771 X18.5) + (0.572 X19.6) + (0.592 AngleA) + (1.834 AngleE) + -291.933	0.91
Y4.7 = (0.143 X6.7) + (0.585 X7.12) + (0.526 X18.7) + (0.307 AngleA) + -23.12627	0.95
Y4.9 = (0.291 X6.9) + (0.687 X16.19) + (-0.653 AngleE) + (0.273 AngleFG) + 67.427	0.73

Equation P_{14}	Rsquared
Y14.5 = (0.442 X5.6) + (0.317 X17.5) + (-1.544 AngleE) + 218.613	0.97
Y14.6 = (-0.334 X5.6) + (0.410 X16.5) + (0.936 X17.6) + (1.095 AngleE) + -147.427	0.96
Y14.7 = (0.269 X6.7) + (1.004 X17.7) + (-0.429 X18.5) + (-1.150 AngleE) + 165.262	0.86
Y14.11 = (0.207 X5.7) + (0.320 X5.10) + (0.896 X16.19) + (-0.381 X17.7) + 30.63603	0.67

Equation P_{15}	Rsquared
Y15.5 = (0.287 X5.6) + (0.813 X1.5) + (0.470 AngleA) + -36.191	0.93
Y15.6 = (0.357 X1.7) + (0.800 X18.6) + (0.585 AngleA) + -62.163	0.91
Y15.7 = (0.252 X6.7) + (0.492 X7.12) + (0.678 X18.7) + (0.612 AngleA) + -58.446	0.86
Y15.9 = (0.173 X5.7) + (0.398 X6.9) + (-0.967 AngleE) + (0.388 AngleFG) + 95.403	0.65

Figure 1

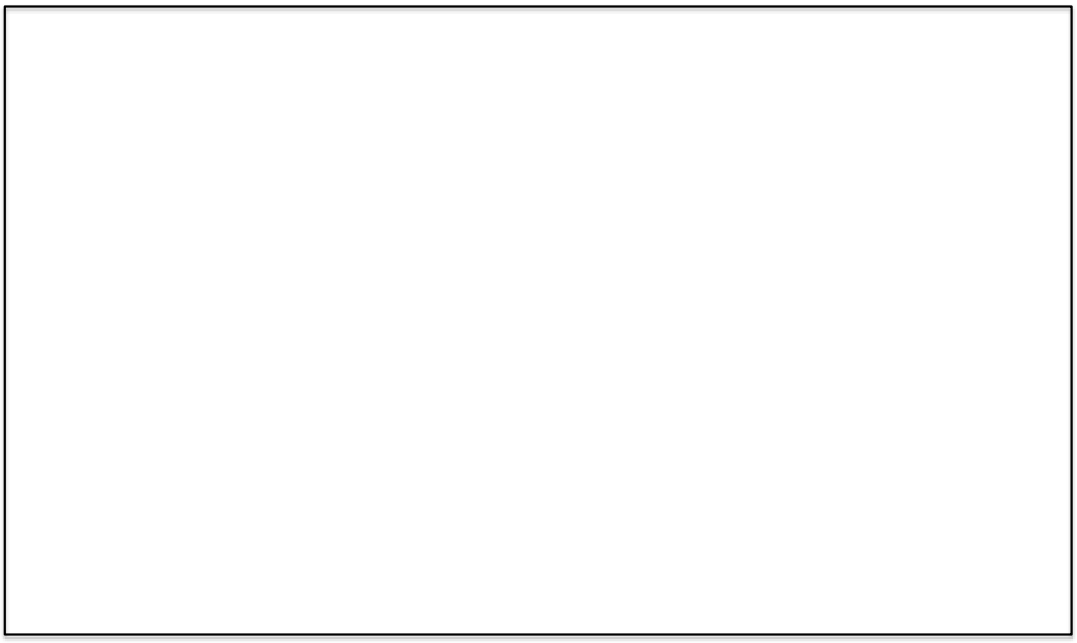

Figure 2